

Phase evolution and thermal stability of high Curie temperature

BiScO₃-PbTiO₃-Pb(Cd_{1/3}Nb_{2/3})O₃ ceramics near MPB

Zhencheng Lan¹, Kaiyuan Chen¹, Xiaofeng He¹, Shuo Zhou¹, Xiande Zheng¹, Jia Liu², Liang Fang¹,
Xiuyun Lei¹, Dawei Wang^{2*}, Biaolin Peng^{3*}, Laijun Liu^{1*}

¹College of Materials Science and Engineering, Guilin University of Technology, Guilin, China

²School of Microelectronics and State Key Laboratory for Mechanical Behaviour of Materials,
Xi'an Jiaotong University, Xi'an, China

³School of Physical Science & Technology and Guangxi Key Laboratory for Relativistic
Astrophysics, Guangxi University, Nanning, China

Abstract: Piezoelectric and ferroelectric ceramics with a high Curie temperature (T_c) have attracted a growing attention owing to their applications under severe environments. In this work, phase structure, dielectric, ferroelectric and piezoelectric properties of $(0.975-x)\text{BiScO}_3-x\text{PbTiO}_3-0.025\text{Pb}(\text{Cd}_{1/3}\text{Nb}_{2/3})\text{O}_3$ ceramics ($x = 0.58-0.64$) were studied. A composition-induced structural transformation occurs from rhombohedral phase to tetragonal phase through an intermediate monoclinic phase with the increasing PT concentration. The relationship between structure and electrical properties of the system were discussed. The BS- x PT-PCN system near the morphotropic phase boundary ($x = 0.62$) exhibits excellent piezoelectric and ferroelectric performances with $d_{33} = 508$ pC/N, $k_p = 56\%$, and $P_r = 40$ $\mu\text{C}/\text{cm}^2$. The high-temperature piezoelectricity of the sample with MPB ($x = 0.62$) was characterized by an *in situ* XRD. The excellent thermal stability of the crystal structure and the piezoelectric property indicate that the BS- x PT-PCN system is a promising candidate for high temperature piezoelectric applications.

*Corresponding authors.

E-mail addresses: dawei.wang@xjtu.edu.cn (Prof. D. Wang), ljliu2@163.com (Prof. L. Liu).

Keywords: High-temperature Piezoelectric Ceramics; Phase structure; Temperature stability

1. Introduction

Materials with excellent piezoelectricity and decent Curie temperature (T_c) are broadly needed for varied applications, for example underwater sonars, automotive, aerospace crafts, etc.,^{1, 2} where they are supposed to function in harsh environments. Nevertheless, majority of the piezoelectrics with excellent piezoelectric properties have a fairly low T_c . For example, $\text{Pb}(\text{Zn}_{1/3}\text{Nb}_{2/3})\text{O}_3\text{-PbTiO}_3$ and $\text{Pb}(\text{Mg}_{1/3}\text{Nb}_{2/3})\text{O}_3\text{-PbTiO}_3$ single crystals have an extremely large piezoelectric constant (d_{33}) of approximately 2500 pC/N^{3, 4, 5, 6, 7} while a low T_c of about 140-170 °C and an even lower T_d of around 60-120 °C, which limits its application temperature range. Consequently, it is an urgent task to find materials with large T_c and excellent performances to adapt to extreme environments.

In the hunt for exquisite perovskite oxides with excellent performances, solid solutions with a morphotropic phase boundary (MPB) have been considered as the most promising candidates. $\text{PbZr}_{1-x}\text{Ti}_x\text{O}_3$ (PZT) ceramics presents the largest dielectric and piezoelectric properties around the MPB for $x=0.48$. Noheda *et al.* found an medium monoclinic (Cm) phase near MPB of PZT⁸ as a structural bridge between the rhombohedral ($R3m$) phase and tetragonal ($P4mm$) phase. This finding created a range of structural investigations on the nature of the morphotropic phase boundary^{9, 10, 11, 12}. Involving studies of the local structure which have illustrated the theory of the decent piezoelectric performances¹³. In spite of the connection between the crystal structure and piezoelectric performance around the MPB has not been adequately comprehend,

the low-symmetry phase is acknowledged to play a vital role in the presence of large piezoelectric performances both in terms of extrinsic¹⁴ and intrinsic contributions¹⁵.

Recently, the $(1-x)\text{BiScO}_3-x\text{PbTiO}_3$ (BS-PT) solid solution have been thoroughly studied, which showed large piezoelectric coefficient ($d_{33} = 460$ pC/N) and high Curie temperature ($T_c > 450$ °C) for the compositions around the MPB ($x = 0.64$)¹⁶. Nevertheless, scandia is too costly to limit the commercial manufacture. Based on Bi-based perovskite piezoelectric ceramics, a number of investigator have take care of $\text{Bi}(\text{Sc}_{3/4}\text{In}_{1/4})\text{O}_3\text{-PbTiO}_3$, $\text{Bi}(\text{Mg}_{1/2}\text{Ti}_{1/2})\text{O}_3\text{-PbTiO}_3$, $\text{Bi}(\text{Sc}_{3/4}\text{Co}_{1/4})\text{O}_3\text{-PbTiO}_3$, $\text{Bi}(\text{Sc}_{1-y}\text{Fe}_y)\text{O}_3\text{-PbTiO}_3$, and $\text{Bi}(\text{Sc}_{1-y}\text{Ga}_y)\text{O}_3\text{-PbTiO}_3$ systems and achieve some satisfactory piezoelectric properties with the T_c beyond 430 °C^{17, 18, 19, 20, 21}. Meanwhile, several researchers attempt to import a third component into the BS-PT binary system to decrease scandia content, for instance, LiNbO_3 , LiTaO_3 ^{22, 23}. The desirable piezoelectric performances were obtained but the T_c reduced significantly, confining their applications at high temperatures. It is known that $\text{Pb}(\text{Cd}_{1/3}\text{Nb}_{2/3})\text{O}_3$ is a classic relaxor ferroelectric material. Previous work²⁴ indicated that $\text{Pb}(\text{Cd}_{1/3}\text{Nb}_{2/3})\text{O}_3$ has two temperatures of dielectric anomaly: the low-temperature one appears at ~33 °C while the high-temperature anomaly happens at about 387 °C. The composition $0.86\text{PbTiO}_3\text{-}0.14\text{Pb}(\text{Cd}_{1/3}\text{Nb}_{2/3})\text{O}_3$, with some appropriately additives, such as MnO_2 , WO_3 , and NiO , shows decent electrical performances and the T_c is exceed 450 °C²⁵. Herein, it is possible to importe $\text{Pb}(\text{Cd}_{1/3}\text{Nb}_{2/3})\text{O}_3$ into the BS-PT system to improve the piezoelectric performances and remain high T_c .

In this work, the phase structure, dielectric, ferroelectric and piezoelectric properties of the PCN-modified BS-PT systems are investigated by modifying the ratio between BS and PT. Since phase stability is vital consideration for high-temperature piezoelectric ceramics, the structure evaluation as a function of temperature was involved to illustrate the nature of the high-temperature piezoelectricity.

2. Experimental procedures

The $(0.975-x)\text{BiScO}_3-x\text{PbTiO}_3-0.025\text{Pb}(\text{Cd}_{1/3}\text{Nb}_{2/3})\text{O}_3$ ceramics (BS- x PT-PCN, $x = 0.58, 0.60, 0.62, 0.64$) were synthesized via the conventional ceramic technology. Analytical grades Sc_2O_3 (99.9%), Bi_2O_3 (99.9%), TiO_2 (99.99%), PbO (99.9%), CdO (99.99%), as well as Nb_2O_5 (99.99%) were selected as the original oxides and were weighed according to the stoichiometric ratio with an extra 2% Bi_2O_3 and PbO to compensate the volatilization of Bi as well as Pb during the sintering stage. The starting materials was ball milled using ethyl alcohol for 12 h, calcined at 800 °C for 4 h in a covered alumina crucible and milled for an added 12 h to make powders uniform and fine. The dried powder was pressed into 10 mm disks at a pressure of 350 MPa. PVA (polyvinyl alcohol) was combusted off at 650 °C for 4 h, then the pellets were surrounded in calcined powder with the uniform composition and sintered at 1080~1100 °C for 2 h in covered crucible.

The phase structure of BS- x PT-PCN was determined via the X-ray diffractometer (XRD, PANalytical, X'Pert PRO) using $\text{Cu } K_\alpha$ radiation from RT to 450 °C. Raman spectroscopy was identified with a 532 nm laser and a valid power of 5.0 mW. The

micromorphology was measured via scanning electron microscopy (SEM, JSM6380-LV, Tokyo, Japan). After the specimens were poled for 30 min in silicon oil bath under a DC field of 70 kV/cm at 120 °C, d_{33} was tested by a piezoelectric d_{33} meter (ZJ-3D, Institute of Acoustics, Beijing, China). Ferroelectric hysteresis loops were collected via Rianant Precision 10 kV HVI-SC analyzer. The dielectric properties dependence on temperature was detected through an impedance analyzer (Agilent 4294A, USA).

3. Results and discussion

3.1 Structure and phase analysis

Figure 1(a) presents XRD patterns of BS- x PT-PCN with different PT contents. All the samples were well crystallized as well as revealed a single perovskite structure no distinctly secondary phases, illustrating that PCN was completely solved into BS-PT lattice. Meanwhile, it is found that the crystalline structure of BS- x PT-PCN ceramics transforms from rhombohedral to tetragonal as the PbTiO_3 content increases. Typical rhombohedral phase can be observed for $x = 0.58$. As x achieves 0.64, the reflection peak (200) has completely split into (002) and (200) peaks, and then the ceramic is a tetragonal phase, as presented in Figure 1(b). The MPB can be identified at $x = 0.62$ parting the rhombohedral phase and tetragonal phase. To further approve the result, the k_p and d_{33} depend on PbTiO_3 content are presented in Figure 2. It can be clearly seen that the d_{33} and k_p intimately depend on PbTiO_3 content, achieving the peak value at $x = 0.62$, which are 56% and 508 pC/N, respectively. The optimal piezoelectric performances are acquired at the composition close to the morphotropic

phase boundary (MPB), which presents a sudden structural transformation ²⁶. Combing with the XRD results, it is considered that the morphotropic phase boundary (MPB) content locates in the vicinity of $x = 0.62$. As reported, the composition of MPB in the pure $\text{BiSO}_3\text{-PbTiO}_3$ ceramics was around the PbTiO_3 content of 0.64 ¹⁶. Obviously, doping with PCN in BS-PT ceramics lead to the MPB composition shifting to lower PbTiO_3 content.

To obtain the structure of the BS- x PT-PCN systems with $x = 0.58, 0.60, 0.62$ and 0.64 , the Rietveld refinements is performed as shown in [Figure 3](#). Details of the refined results were cataloged in [Table 1](#). The samples with $x = 0.58$ and $x = 0.60$ are under the threshold boundary of phase coexistence (resulting in the MPB) and the symmetry is rhombohedral with the space group $R3m$. For the composition at $x = 0.64$, a single tetragonal phase with space group $P4mm$ was used to refine the XRD pattern, resulting in good agreement.

On the other hand, phase coexistence was clearly observed for the composition $x = 0.62$. The best R factors were obtained in the case of a heterogeneous model embracing tetragonal $P4mm$ and monoclinic Cm phase ([Table 1](#), [Figure 3](#)). Such presence of an intermediate monoclinic phase, which divides the rhombohedral and the tetragonal region on the x -T phase diagram, was first proposed for the by Noheda *et al* ⁸ for PZT ceramics. Later, a similar phase was discovered during the investigation of the BS-PT ^{27, 28} ceramics. Given these pioneering work, the presence of the monoclinic phase and the existence of MPB in the ternary system BS- x PT-PCN is expected.

Figure 4(a) presents Raman spectra taken at room temperature for the BS- x PT-PCN samples with $x = 0.58, 0.60, 0.62$ and 0.64 . The Raman spectra were deconvoluted using a Gaussian-Lorentzian mixed profile as plotted in Figure 4(b). Composition dependence of the Raman shift is revealed in Figure 4(c). The $A_1(1LO)$, and $E(2TO)$ peaks between 200 cm^{-1} and 450 cm^{-1} , corresponding to the Ti-O and Sc-O bond vibrations⁴⁰. A sudden change in Raman shifts of the two peaks around $x = 0.62$ could be related to the phase transition from rhombohedral to tetragonal, which agrees with the XRD results.

Figure 5 presents SEM images of the BS- x PT-PCN ($x = 0.58-0.64$) ceramics. The SEM photos exhibit that all the samples are dense with well-grown grain. The component of $x = 0.62$ has the smallest grain size. Meanwhile the average grain size of the BS- x PT-PCN system is approximately $2.17\sim 2.44\ \mu\text{m}$. The change of x has no prominent impact on the grain size of the system. The dense and uniform morphology is fundamental for the ceramics to have excellent mechanical performances.

3.2 Dielectric behavior

Figure 6(a)-(d) show temperature as a function of dielectric performances (ϵ_r , $\tan\delta$) of the BS- x PT-PCN ceramics. It can be obviously seen that the T_c nearly linearly increases from $366\text{ }^\circ\text{C}$ to $420\text{ }^\circ\text{C}$ with the increase of x . For the MPB composition, the T_c achieves $401\text{ }^\circ\text{C}$, which is a bit lower than that of pure $\text{BiScO}_3\text{-PbTiO}_3$ ²⁹. The loss tangent ($\tan\delta$) of all specimens is lower than 0.08 from RT to $350\text{ }^\circ\text{C}$ at 1 kHz , which illustrates that BS- x PT-PCN is potentially appropriate for harsh environment. The shape of dielectric permittivity peaks become suppressed and broader with the lower

PbTiO₃ contents, which belongs to diffuse phase transition behavior. The diffuse phase transformation is often ascribed to the balance breaking of component and structural disorder in the arrangement of non-isovalent Nb⁵⁺ and Cd²⁺ ions on the crystallographic equivalent sites.

For purpose of illustrate the dielectric relaxor behavior of the BS-*x*PT-PCN (*x* = 0.58-0.64) ceramics, we used the quadratic Lorentz formula: ³⁰

$$\frac{\varepsilon_A}{\varepsilon} = 1 + \frac{(T - T_A)^2}{2\delta_A^2} \quad (1)$$

where T_A and ε_A are the temperature of the dielectric peak and the speculative value of ε_A at $T = T_A$, respectively. The coefficient δ_A represents the diffuseness of the dielectric peak. The greater is the relaxor dispersion, the larger is δ_A . The temperature as a function of the dielectric permittivity at $T > T_m$ for BS-*x*PT-PCN ceramics was fitted by Eq. (1) as presented in [Figure 6](#). As the fitting parameters ([Table 3](#)) indicate, it can be obviously seen that the parameter δ_A decreases as the PT content increased, implying the degree of diffusion phase transition decreases. which is related to a small amount of the Cd and Nb occupying the B site in the perovskite structure, leading to the B site ion distribution becoming disordered ³¹.

Frequency dispersion of the phase transition in ferroelectric materials can be described by the Vogel-Fulcher formula, which introduces the concept of "freezing temperature" and reflects the freezing process caused by the interaction between dipoles or polar nanoregions (PNRs). The relationship of the Vogel-Fulcher can be described as follows:

$$f = f_0 \exp(-E_a / k_B(T_m - T_f)) \quad (2)$$

where f_0 is the frequency of tries to conquer the potential barrier E_a ($f_0 \sim 10^{13}$, in our case); k_B is the Boltzmann constant; T_f is the static freezing temperature. Figure 7 presents the T_m dependence of f . The obtained E_a , T_f and f_0 are cataloged in Table 3. T_f ascends from 590 to 678 K with PbTiO_3 increasing from 0.58 to 0.64, illustrating the presence of freezing behavior in the dipole dynamics upon RT³². The calculated E_a is around 0.022~0.069 eV, E_a gradually decreased with the increase of PT, indicating that the interaction between PNRs increased.

3.3 Piezoelectric and ferroelectric properties

The P - E hysteresis loops of the specimens are presented in Figure 8(a). All the polarized samples exhibit saturated P - E loops under driven fields. Figure 8(b) demonstrates the composition dependence of the coercive field (E_c) and the remnant polarization (P_r). With the increase of x , the P_r initially increases, attains the maxima $40 \mu\text{C}/\text{cm}^2$ around the MPB ($x = 0.62$), then decreases to $\sim 28 \mu\text{C}/\text{cm}^2$ for $x = 0.64$. This should be attributed to facilitated polarization by phase coexistence, where monoclinic phase equipped twenty four spontaneous polarization directions and six autonomous polarization directions for tetragonal phase, giving a sum thirty directions³³. The highest ferroelectric property was obtained at the MPB content $x = 0.62$ with a coercive field $E_c = 19.6 \text{ kV}/\text{cm}$ and remnant polarization $P_r = 40 \mu\text{C}/\text{cm}^2$. The E_c first reduces slightly to $19.6 \text{ kV}/\text{cm}$, and then increases to $25.9 \text{ kV}/\text{cm}$. This is consistent with the XRD results since the domain switching getting harder with the increase fraction of the tetragonal phase. As exhibited in Table 2, Figure 2 and Figure 8, the change tendency of piezoelectric parameter d_{33} is analogous to that of P_r and ϵ , which

can be revealed as follows: d_{33} is proportional to $Q\varepsilon_0\varepsilon P_r$ ³⁴, where Q , ε_0 , ε as well as P_r represent the electrostriction coefficient, dielectric parameter of vacuum, dielectric permittivity as well as remnant polarization of samples, respectively.

3.4 Temperature as a function of depoling and phase structure of BS- x PT-PCN ceramics

Figure 9(a) and (b) show the thermal stability of d_{33} and k_p from RT to 400 °C of the BS- x PT-PCN system. The piezoelectric coefficient maintains decent stability, meanwhile, harsh deterioration of the piezoelectric properties does not happen until near the T_c . To further shed light on the connection between the deterioration of piezoelectric characterization and depoling temperature, an *in situ* XRD of the BS-0.62PT-PCN was accomplished from RT to 450 °C as plotted in Figure 10(a). Figure 10(b) presents the variation of the phase fraction of monoclinic, tetragonal and cubic dependence on temperature. In the temperature region RT to 250 °C, the BS-0.62PT-PCN mainly sustains its tetragonal phase, revealing high thermal stability of vertical MPB. Hence, the piezoelectric performances of BS-0.62PT-PCN present good temperature stability ascribed to the phase fraction maintains unchanged. It is consistent with the dielectric behavior and annealing test of d_{33} . Further increasing temperature, the appearance of cubic phase around 400 °C implies an evident phase transformation from ferroelectric to paraelectric happens. As a result, the d_{33} and k_p degenerates to zero around the T_c . Consequently, the reason of excellent piezoelectric performance of the BS- x PT-PCN ceramics around MPB is ascribed to the low symmetry monoclinic phase (where the switching of polarization is easy) while the

decent high-temperature thermal stability is attributed to the good stability of tetragonal and monoclinic phases. The results validate that BS- x PT-PCN ceramics are a promising candidate for high temperature piezoelectric applications.

4. Conclusions

The BS- x PT-PCN ceramics ($0.58 \leq x \leq 0.64$) were manufactured by the traditional solid state reaction method. The phase structure, microstructure as well as electrical performances of the BS- x PT-PCN ceramics were investigated. The increase of PT results in a structural phase transformation from rhombohedral phase to tetragonal phase. The vicinity of MPB ($x = 0.62$) is demonstrated by a mixture of phases: monoclinic phase (space group, Cm) and tetragonal phase (space group, $P4mm$). The ceramic with $x = 0.62$ indicates optimal dielectric, piezoelectric, and ferroelectric performances with $\epsilon_{rmax} = 31565$, $T_c = 401$ °C, $d_{33} = 508$ pC/N, $k_p = 56\%$, and $P_r = 40$ μ C/cm². With a higher T_c than merchant PZT ceramics, BS- x PT-PCN ceramics exhibit excellent piezoelectric parameter of 508 pC/N, which is higher than d_{33} (460 pC/N) of pure BS-PT ceramics. Thermal depoling on piezoelectric properties dependence on temperature indicates a decent temperature stability. It is considered that the BS- x PT-PCN ceramics are promising for application as high-temperature sensors and actuators.

Acknowledgments

This work was financially supported by the Natural Science Foundation of China (NSFC Grant Nos. 11564010, 51402196, 51602159). D.W. acknowledges the support of NSFC (Grant Nos. 11574246 and U1537210) and the National Basic Research

Program of China, Grant No. 2015CB654903. L.L also thanks the support from the Natural Science Foundation of Guangxi (Grant No. GA139008, AA138162, CB380006, FA198015), the Research Grants Council of the Hong Kong Special Administrative Region, China (ProjectNo.PolyU152665/16E), the Scientific Research Foundation of Guangxi University (GrantXTZ160530).

Reference

- ¹J. Chen, G. Jin, C.-M. Wang, J. Cheng, and D. Damjanovic, *J. Am. Ceram. Soc.* **97**, 3890 (2014).
- ²Z. Dai, W. Liu, D. Lin, and X. Ren, *Mater. Lett.* **215**, 46 (2018).
- ³X. Zhao, J. Wang, K.-H. Chew, H. L.-W. Chan, C.-L. Choy, Z. Yin, and H. Luo, *Mater. Lett.* **58**, 2053 (2004).
- ⁴K. K. Rajan and L. C. Lim, *Appl. Phys. Lett.* **83**, 5277 (2003).
- ⁵S. Zhang, L. Lebrun, D. Y. Jeong, C. A. Randall, Q. Zhang, and T. R. ShROUT, *J. Appl. Phys.* **93**, 9257 (2003).
- ⁶S. Zhang, J. Luo, W. Hackenberger, N. P. Sherlock, R. J. Meyer, Jr, and T. R. ShROUT, *J. Appl. Phys.* **105**, 104506 (2009).
- ⁷D. Viehland, J. Powers, L. E. Cross, and J. F. Li, *Appl. Phys. Lett.* **78**, 3508 (2001).
- ⁸B. Noheda, D. E. Cox, G. Shirane, J. A. Gonzalo, L. E. Cross, and S. E. Park, *Appl. Phys. Lett.* **74**, 2059 (1999).
- ⁹J. Frantti, S. Ivanov, S. Eriksson, H. Rundlöf, V. Lantto, J. Lappalainen, and M. Kakihana, *Phys. Rev. B.* **66** (2002).
- ¹⁰D. Phelan, X. Long, Y. Xie, Z. G. Ye, A. M. Glazer, H. Yokota, P. A. Thomas, and P. M. Gehring, *Phys. Rev. Lett.* **105**, 207601 (2010).
- ¹¹N. Zhang, H. Yokota, A. M. Glazer, and P. A. Thomas, *Acta Crystallogr. B.* **67**, 386 (2011).
- ¹²S. Gorfman, D. S. Keeble, A. M. Glazer, X. Long, Y. Xie, Z. G. Ye, S. Collins, and P. A. Thomas, *Phys. Rev. B.* **84** (2011).

- ¹³N. Zhang, H. Yokota, A. M. Glazer, Z. Ren, D. A. Keen, D. S. Keeble, P. A. Thomas, and Z. G. Ye, *Nat. Commun.* **5**, 5231 (2014).
- ¹⁴J. L. Jones, M. Hoffman, J. E. Daniels, and A. J. Studer, *Appl. Phys. Lett.* **89**, 092901 (2006).
- ¹⁵H. Fu and R. E. Cohen, *Nature*. **403**, 281 (2000).
- ¹⁶E. E. Richard, A. R. Clive, R. S. Thomas, W. R. Paul, W. Hackenberger, and S. E. Park, *Jpn. J. Appl. Phys.* **40**, 5999 (2014).
- ¹⁷Z. Hu, J. Chen, M. Li, X. Li, G. Liu, and S. Dong, *J. Appl. Phys.* **110**, 064102 (2011).
- ¹⁸Q. Zhang, Z. Li, F. Li, Z. Xu, and X. Yao, *J. Am. Ceram. Soc.* **93**, 3330 (2010).
- ¹⁹Z. Yao, H. Liu, Y. Liu, Z. Li, X. Cheng, M. Cao, and H. Hao, *Mater. Lett.* **62**, 4449 (2008).
- ²⁰I. Sterianou, D. C. Sinclair, I. M. Reaney, T. P. Comyn, and A. J. Bell, *J. Appl. Phys.* **106**, 12 (2009).
- ²¹E. D. Politova, G. M. Kaleva, A. V. Mosunov, and A. H. Segalla, *Phys. Scripta.* **89**, 044007 (2014).
- ²²Y. Chen, J. Zhu, D. Xiao, B. Qin, and Y. Jiang, *J. Alloy. Compd.* **470**, 420 (2009).
- ²³Y. Zhao, Y. Jiang, and J. Zhu, *Phys. Stat. Sol. A.* **207**, 199 (2010).
- ²⁴W. Bąk, C. Kajtoch, K. Mroczka, and K. Wójcik, *Arch. Mater. Sci. Eng.* **33**, 75 (2008).
- ²⁵J. Shenglin, W. Xiaozheng, and Z. Xuli, *Ferroelectrics.* **197**, 155 (1997).
- ²⁶Y. Saito, H. Takao, T. Tani, T. Nonoyama, K. Takatori, T. Homma, T. Nagaya, and M.

- Nakamura, Nature. **432**, 84 (2004).
- ²⁷J. Chaigneau, J. M. Kiat, C. Malibert, and C. Bogicevic, Phys. Rev. B. **76** (2007).
- ²⁸K. Datta, D. Walker, and P. A. Thomas, Phys. Rev. B. **82** (2010).
- ²⁹R. E. Eitel, C. A. Randall, T. R. ShROUT, and S.-E. Park, Jpn. J. Appl. Phys. **41**, 1347 (2002).
- ³⁰J. Deng, X. Sun, S. Liu, L. Liu, T. Yan, L. Fang, and B. Elouadi, J. Adv. Dielectr. **06**, 1650009 (2016).
- ³¹L. Liu, M. Knapp, H. Ehrenberg, L. Fang, H. Fan, L. A. Schmitt, H. Fuess, M. Hoelzel, H. Dammak, M. P. Thi, and M. Hinterstein, J. Eur. Ceram. Soc. **37**, 1387 (2017).
- ³²N. Raengthon, T. Sebastian, D. Cumming, I. M. Reaney, D. P. Cann, and J. Roedel, J. Am. Ceram. Soc. **95**, 3554 (2012).
- ³³V. A. Isupov, Sov. Phys. Sol. St, USSR. **12**, 1084 (1970).
- ³⁴S.-E. Park and T. R. ShROUT, J. Appl. Phys. **82**, 1804 (1997).
- ³⁵M. V. Talanov, A. A. Bush, K. E. Kamentsev, V. P. Sirotinkin, and A. G. Segalla, J. Am. Ceram. Soc. **101**, 683 (2018).
- ³⁶B. Deng, Q. Wei, C. He, Z. Wang, X. Yang, and X. Long, J. Alloy. Compd. **790**, 397 (2019).
- ³⁷T.-H. Song, R. E. Eitel, T. R. ShROUT, C. A. Randall, and W. Hackenberger, Jpn. J. Appl. Phys. **42**, 5181 (2003).
- ³⁸Q. Hu, Y. Wang, L. Wu, J. Yin, L. Chen, G. Yuan, and Y. Yang, J. Mater. Sci-Mater. El. **29**, 18036 (2018).

³⁹S. Zhang, L. Lebrun, S. Rhee, R. E. Eitel, C. A. Randall, and T. R. ShROUT, *J. Cryst. Growth.* **236**, 210 (2002).

⁴⁰A. A. Bokov and Z. G. Ye, *Sol. St. Comm.* **116**, 105 (2000).

Table 1 Results of the Rietveld refinement of the sample with $x = 0.58, 0.60, 0.62$ and 0.64 at RT.

PbTiO ₃ content	$x = 0.58$	$x = 0.60$	$x = 0.62$	$x = 0.64$	
Space group	<i>R3m</i>	<i>R3m</i>	<i>P4mm</i>	<i>Cm</i>	<i>P4mm</i>
Phase fraction	1	1	0.732	0.268	1
<i>a</i>	4.03302(0)	4.02739(3)	3.99367(4)	5.67819(2)	3.99217(7)
<i>b</i>	4.03302(0)	4.02739(3)	3.99367(4)	5.66168(8)	3.99217(7)
<i>c</i>	4.03302(0)	4.02739(3)	4.06155(5)	4.04328(1)	4.07647(7)
β	89.8176	89.8742	90.0000	89.8007	90.000
Cell volume (Å ³)	65.609	65.323	64.780	130.711	64.971
Bi/Pb					
<i>x</i>	0.5	0.5	0	0	0
<i>y</i>	0.5	0.5	0	0	0
<i>z</i>	0.5	0.5	0	0	0
Ti					
<i>x</i>	0.0466820	0.046700	0.5	0.480000	0.5
<i>y</i>	0.0466820	0.046700	0.5	0	0.5
<i>z</i>	0.0466820	0.046700	0.524000	0.656030	0.52368
Sc					
<i>x</i>	0.046682	0.046700	0.5	0.480000	0.5
<i>y</i>	0.046682	0.046700	0.5	0	0.5
<i>z</i>	0.046682	0.046700	0.524000	0.656030	0.524000
Nb					
<i>x</i>	0.046682	0.046700	0.5	0.480000	0.5
<i>y</i>	0.046682	0.046700	0.5	0	0.5
<i>z</i>	0.046682	0.046700	0.524000	0.656030	0.524000
Cd					
<i>x</i>	0.046682	0.046700	0.5	0.480000	0.5
<i>y</i>	0.046682	0.046700	0.5	0	0.5
<i>z</i>	0.046682	0.046700	0.524000	0.656030	0.524000
O1					
<i>x</i>	0.552410	0.551200	0.5	0.457110	0.5
<i>y</i>	0.065260	0.066500	0.5	0	0.5
<i>z</i>	0.065260	0.066500	0.123000	0.031670	0.123000
O2					
<i>x</i>			0.5	0.225660	0.5
<i>y</i>			0	0.252280	0

z			0.584000	0.543610	0.584000
R_{wp}	0.0640	0.0639	0.0635		0.0788
R_p	0.0461	0.0452	0.0450		0.0515
χ^2	4.861	4.657	5.597		6.995

Table 2 Room temperature dielectric and piezoelectric properties of BS- x PT-PCN ceramics.

Composition	ϵ_{rmax}	$\tan \delta$	T_c (°C)	d_{33} (pC/N)	K_p	P_r ($\mu\text{C}/\text{cm}^2$)	E_c (kV/cm)	
$x = 0.58$	16990	0.0313	366	256	0.41	28	21.7	
$x = 0.60$	19103	0.0307	380	375	0.50	30	17.8	
$x = 0.62$	31565	0.0289	401	508	0.56	40	19.6	
$x = 0.64$	26562	0.0237	420	244	0.38	27	25.9	
BS-0.42PT-0.42PMN	11110	0.0660	102	509	0.46	28	12	[35]
BS-0.64PT-0.03PMS		0.0075	365	300	0.43	22	17	[36]
BS-0.58PT-0.06BST		0.05	384	440	0.46	29	20	[37]
BS-0.61PT-0.03LN		0.0073	337	551	0.51	46.5	23	[38]
BS-0.64PT		0.020	450	460	0.56	32	20	[39]

Table 3 Fitting parameters for different compositions of BS- x PT-PCN solid solution obtained using Vogel-Fulcher law and quadratic Lorentz.

Compositio n	T_f (K)	f_0 (Hz)	E_a (eV)	T_A (K)	δ_A (K)	ϵ_A
$x = 0.58$	590	1.50×10^{13}	0.069	611	88	15514
$x = 0.60$	614	1.86×10^{13}	0.058	633	82	17599
$x = 0.62$	630	1.79×10^{13}	0.054	647	64	28197

Figure Captions

Fig. 1 (a) XRD patterns (b) magnified XRD profiles of {200} of the BS- x PT-PCN ($0.58 \leq x \leq 0.64$) ceramics.

Fig. 2 Piezoelectric coefficient d_{33} and planar electromechanical coupling factor k_p for BS- x PT-PCN at RT.

Fig. 3 Rietveld refinement for the BS- x PT-PCN ($x = 0.58, 0.60, 0.62, 0.64$) ceramics at RT.

Fig. 4 (a) Room temperature Raman spectra, (b) Fitting spectra and (c) The change of peak positions based on the fitting results of Raman spectra for the BS- x PT-PCN system with different compositions.

Fig. 5 SEM micrographs of the BS- x PT-PCN ceramics: (a) $x = 0.58$; (b) $x = 0.60$; (c) $x = 0.62$; (d) $x = 0.64$. Insert shows the grain size distribution of BS- x PT-PCN ceramics.

Fig. 6 Temperature dependence of dielectric properties (ϵ_r , $\tan\delta$) of the BS- x PT-PCN ($0.58 \leq x \leq 0.64$) ceramics. Plots of quadratic Lorentz fittings of the temperature dependence of the dielectric permittivity at 100 kHz.

Fig. 7 The results of Vogel-Fulcher fitting for the BS- x PT-PCN ceramics with $x = 0.58, 0.60, 0.62, 0.64$.

Fig. 8 (a) Polarization hysteresis loops of the BS- x PT-PCN ceramics (b) The P_r and E_c of the ceramics with different x .

Fig. 9 Effect of thermal depoling on the (a) piezoelectric parameter d_{33} and (b) planar electromechanical coupling factor k_p of the BS- x PT-PCN ceramics.

Fig. 10 (a) Structural phase transition as a function of temperature for $x = 0.62$. A selected range of 2θ shows the transformation of the $\{200\}$ Bragg Reflection with the temperature. (b) tetragonal and monoclinic phase fractions as a function of temperature.

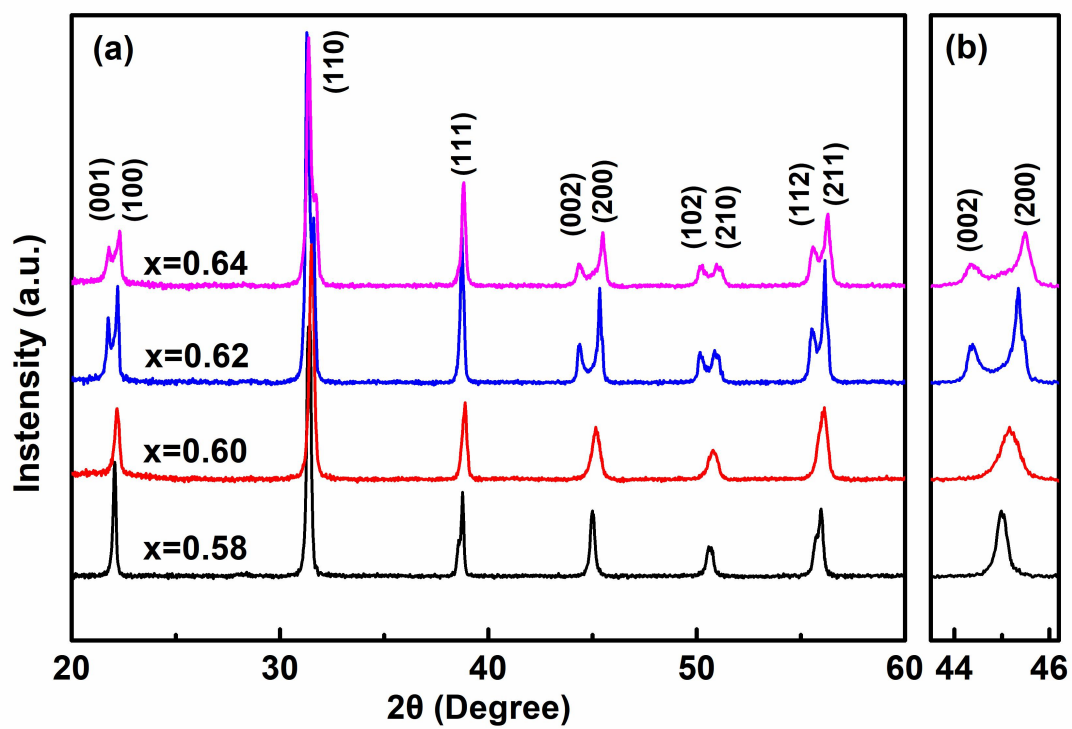


Fig. 1

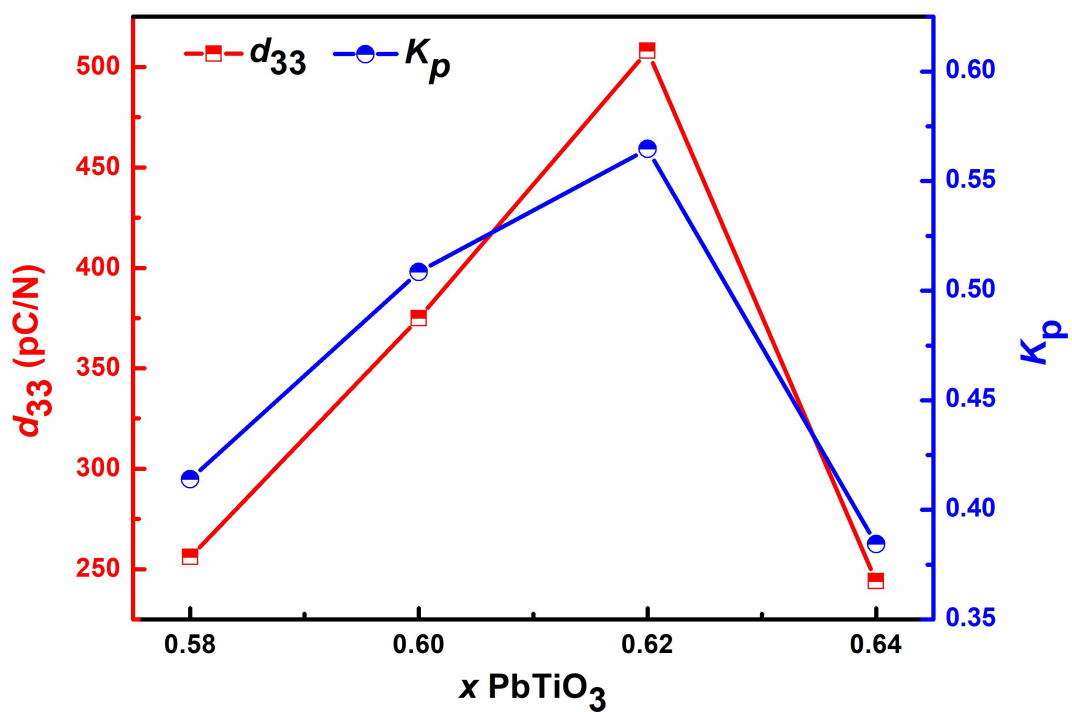


Fig. 2

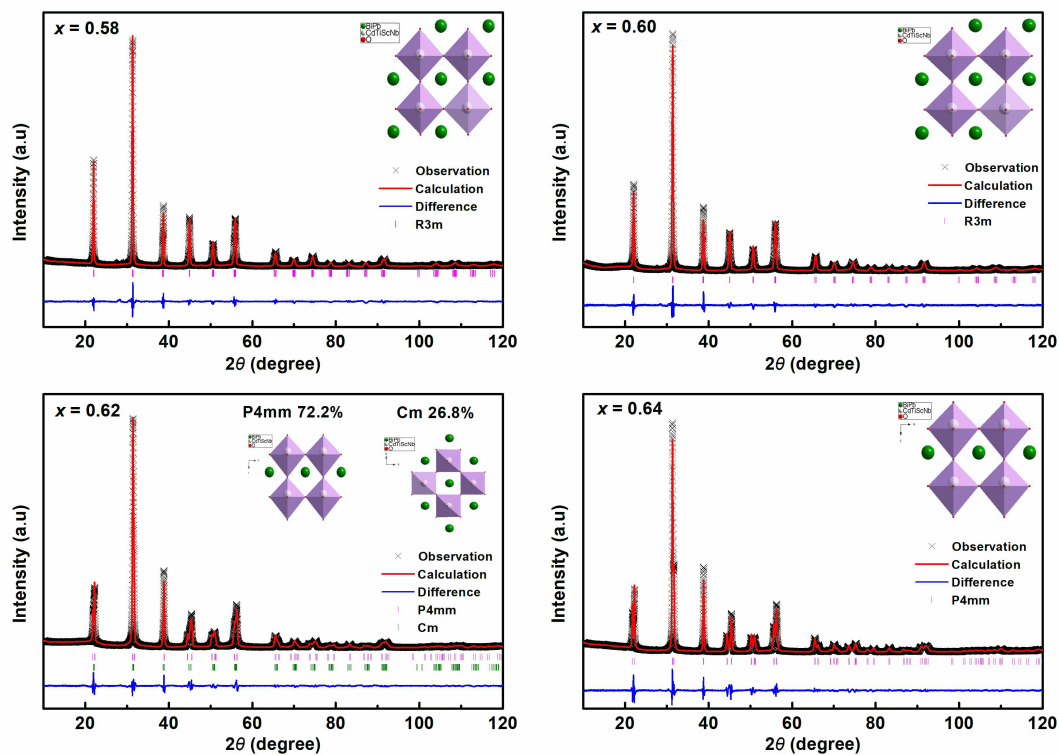


Fig. 3

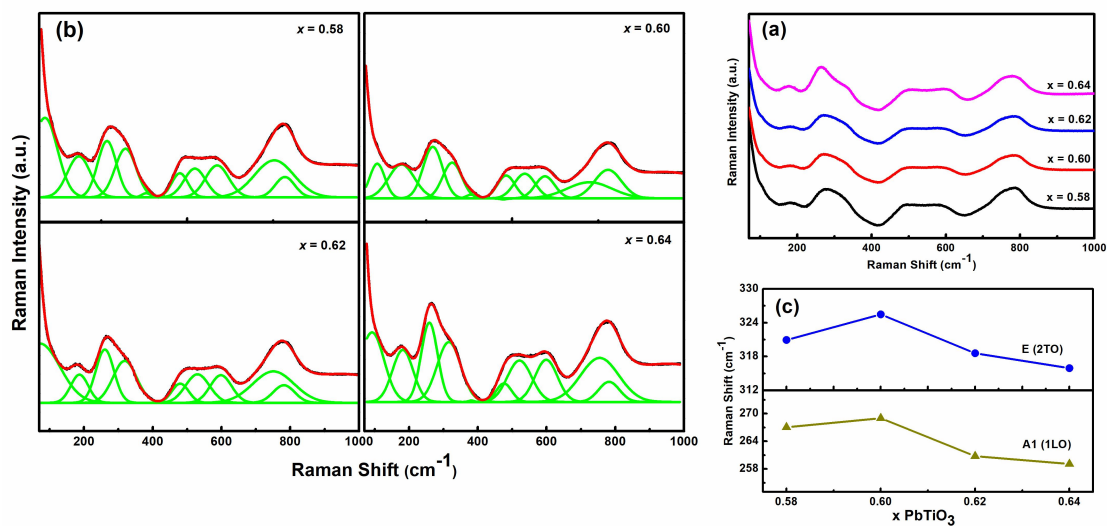


Fig. 4

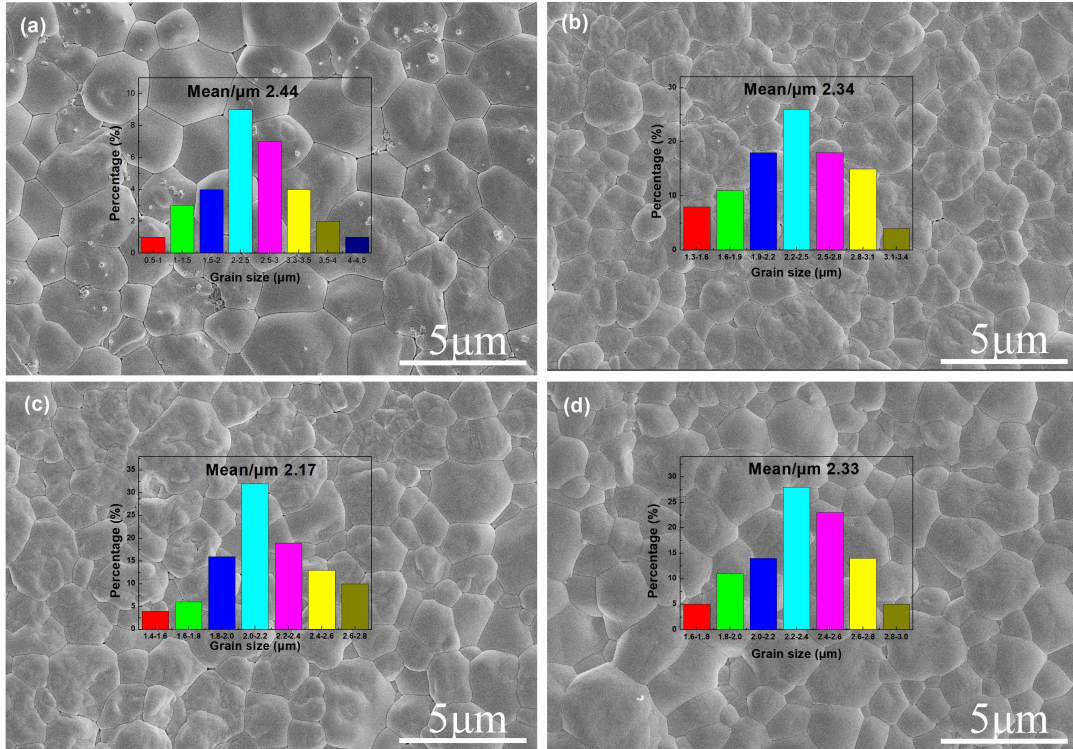


Fig. 5

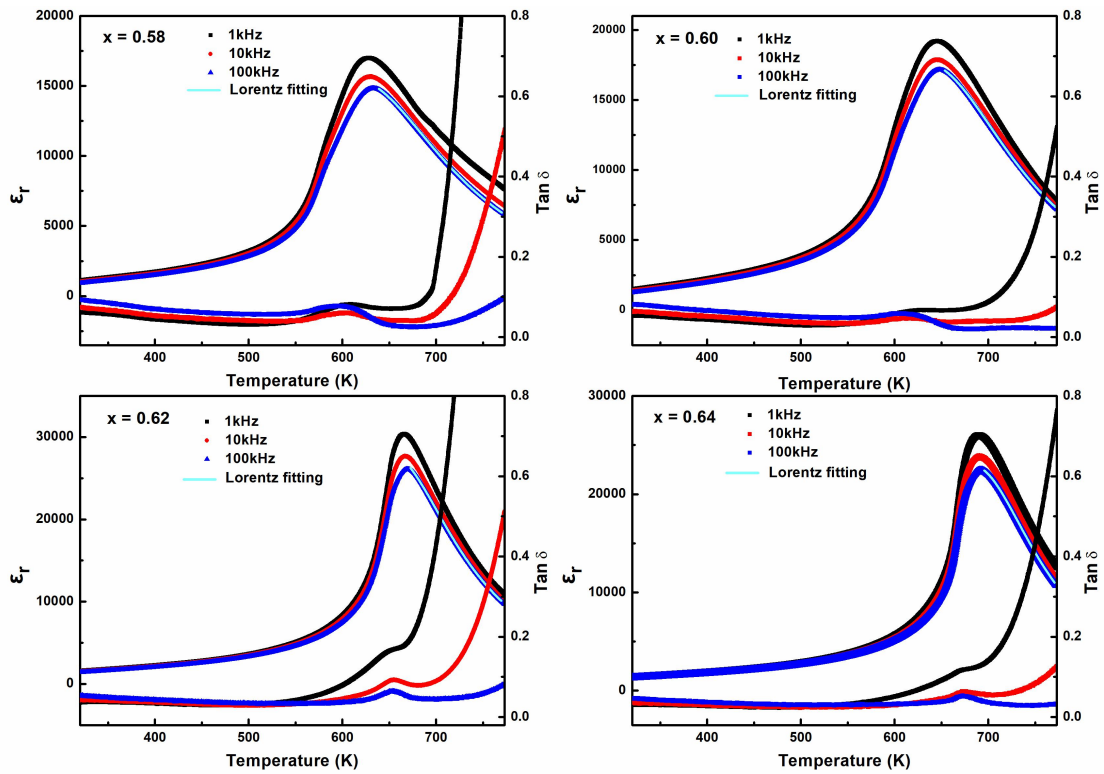


Fig. 6

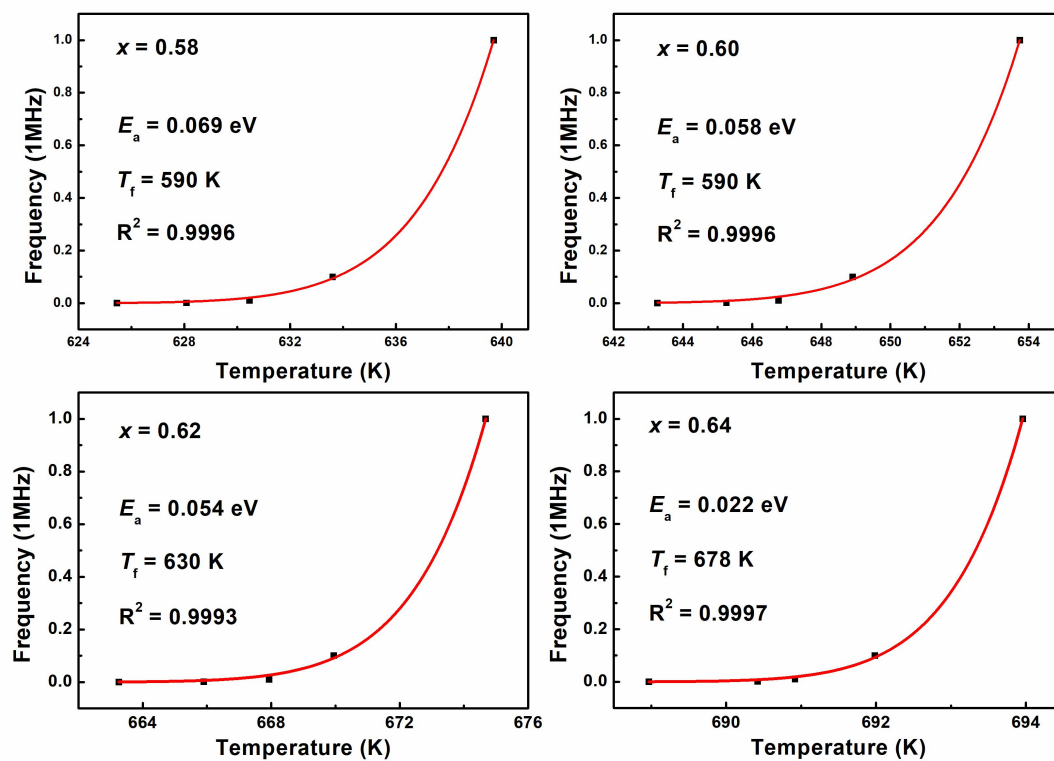
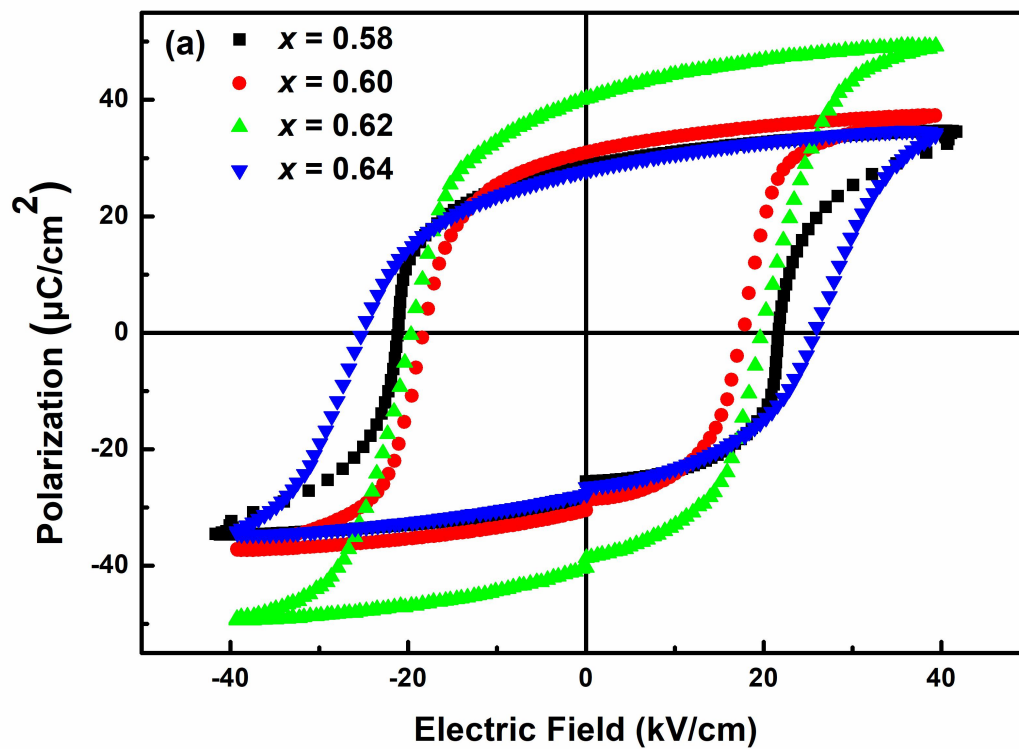


Fig. 7



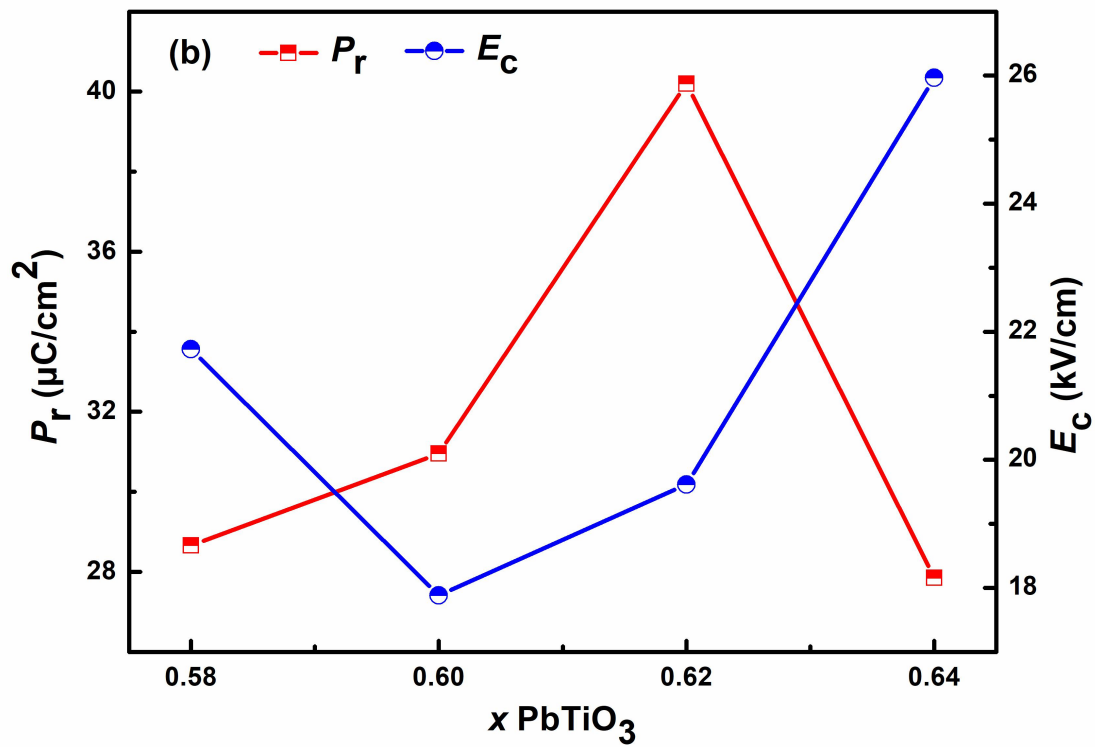
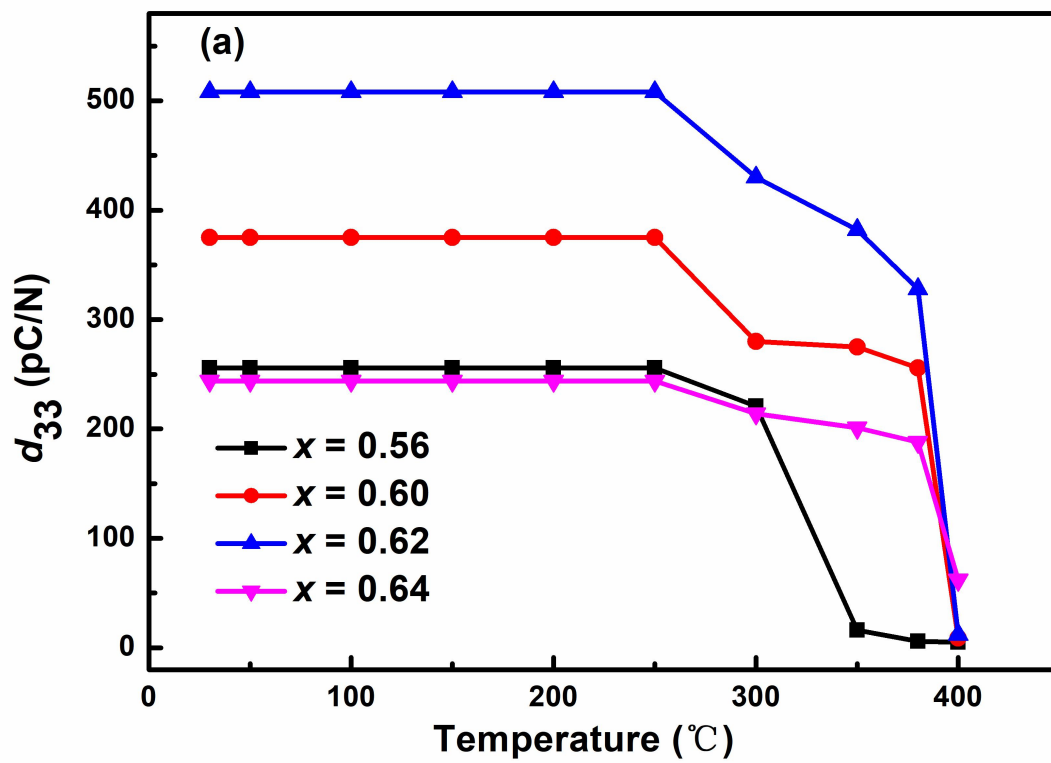


Fig. 8



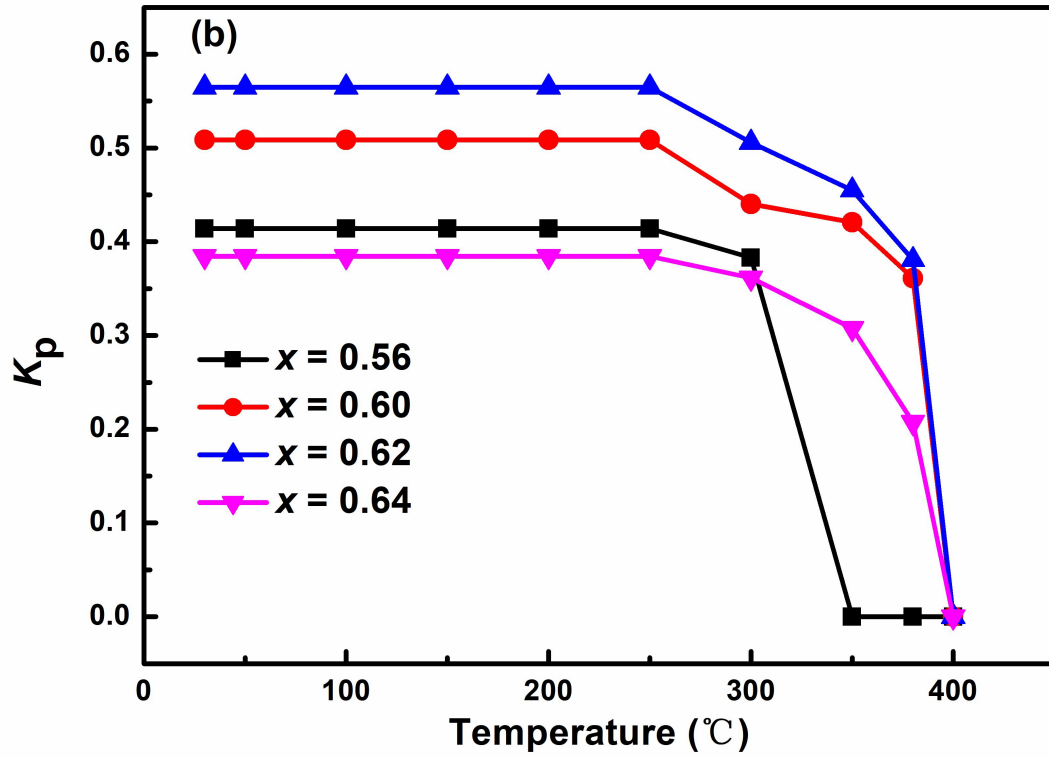
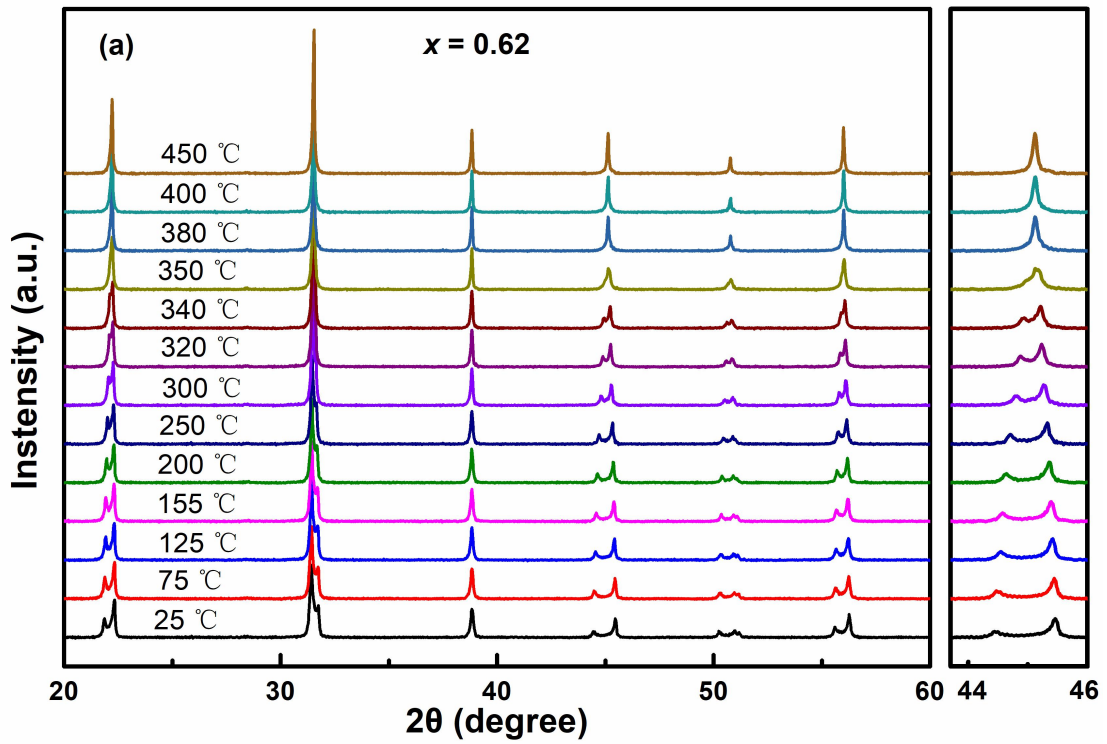


Fig. 9



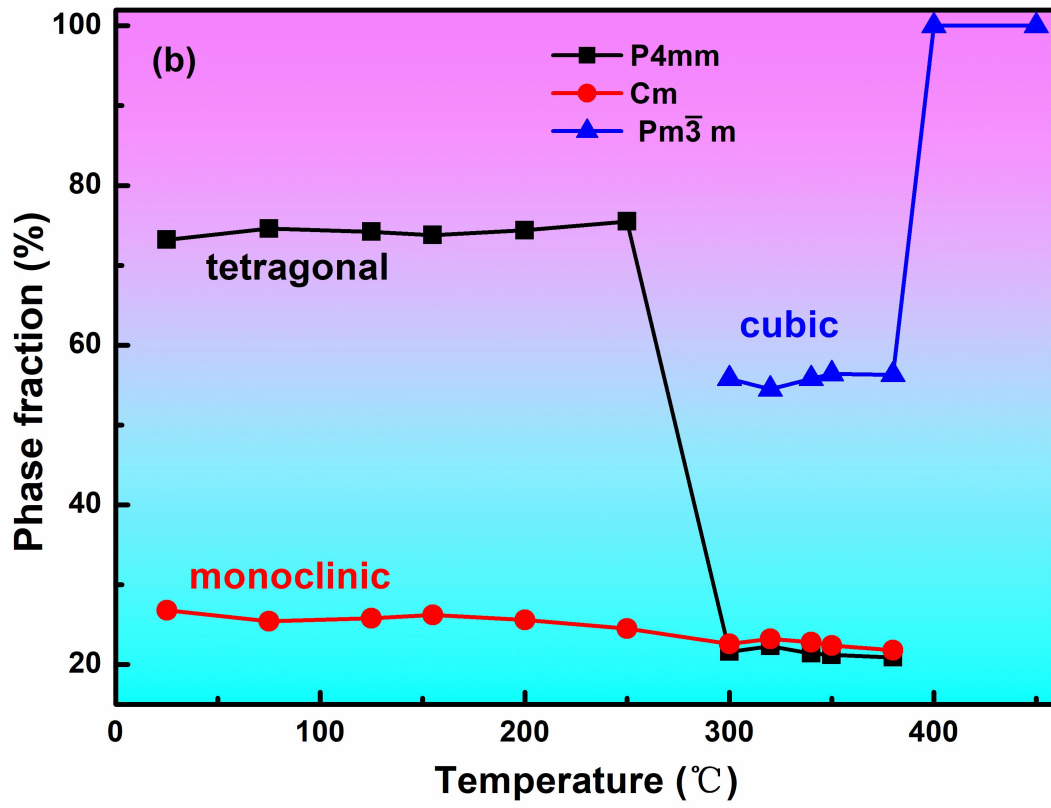


Fig. 10